Improving edge recovery in udersampled MRI reconstruction

Zhong Chen[1], Changwei Hu[1], Xiaobo Qu[1], Lijun Bao[1], and Shuhui Cai[1]

[1]*Department of Electronic Science, Fujian Key Laboratory of Plasma and Magnetic Resonance, Xiamen University, Xiamen, Fujian, China, People's Republic of*

Introduction

In MRI, significant aliasing artifacts are introduced when the k-space is highly undersampled, which blur the reconstructed edges. The edges usually contain useful morphological information for the diagnosis of focal areas, such as the margin of the tumor, and the caliber of the vessel. Therefore, undersampled MRI reconstruction with good edge recovery is important for clinical diagnosis. In this work, we define a weighting matrix from an edge scoring function to obtain better edge recovery. The edge scoring function is designed by considering the strength, orientation, and spatial continuity of the edge features in local patches in à trous wavelet domain. Simulations indicate that the proposed method yields reconstructions with better edge recovery than conventional compressed sensing methods, and requires fewer k-space measurements to achieve reconstruction error of the same level.

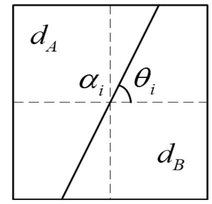

Fig. 1 The strength and orientation of the edge.

Methods

The reconstruction formulation for the proposed method is $\min_{\boldsymbol{\alpha}} \|\mathbf{y}-\mathbf{F}_u\boldsymbol{\Psi\alpha}\|_2^2/2+\lambda\|\mathbf{W}\boldsymbol{\alpha}\|_1$, where $\boldsymbol{\Psi}$ is the sparsifying transform (à trous wavelet in this work), $\mathbf{y}$ is measured k-space data, $\boldsymbol{\alpha}$ is the sparse representation of a $N\times1$ signal $\mathbf{x}$ ($\mathbf{x}=\boldsymbol{\Psi\alpha}$) produced by vectorizing the magnetic resonance image. $\mathbf{F}_u$ represents undersampled Fourier transform, λ is a regularization parameter governing the tradeoff between the data consistency and sparsity. $\mathbf{W}$ is a weighting matrix generated from the edge scoring function $f(\cdot)$ by $\mathbf{W}=1/f(\cdot)$. $f(\cdot)$ is designed by combining two components $f(\cdot)=I(\cdot)\cdot C(\cdot)$, where the first component $I((x_{\alpha_i},y_{\alpha_i}),\Delta\theta_i)=\sqrt{x_{\alpha_i}^2+y_{\alpha_i}^2}\cdot(\cos(\Delta\theta_i)+1)$ is used to quantify the contribution of wavelet coefficient α_i to the edge features in the local patch, while the second component $C((x_{\alpha_i},y_{\alpha_i}),(x_{pat},y_{pat}))=\sqrt{(x_{pat}-x_{\alpha_i})^2+(y_{pat}-y_{\alpha_i})^2}$ is used to measure the spatial continuity of edge features passing through α_i. $(x_{\alpha_i},y_{\alpha_i})$ and (x_{pat},y_{pat}) are two vectors defined based on the strenth and orientation of the edge in a local patch, and $\Delta\theta_i$ is the angle between $(x_{\alpha_i},y_{\alpha_i})$ and (x_{pat},y_{pat}). The strength and orientation of the edge is defined as follows. Suppose a square-shaped window centered at wavelet coefficient α_i is divided into two sub-windows by a line with angle θ_i ($0\le\theta_i<\pi$), as shown in Fig. 1. Let the sum of the coefficients in the two sub-windows be d_A and d_B. The edge strength d_{α_i}, which reflects the intensity transition of wavelet coefficients along the edge, is defined by the maximal difference between d_A and d_B as θ_i changes, and the angle θ_i is defined as the directional orientation of the edge at α_i. Then $(x_{\alpha_i},y_{\alpha_i})$ and (x_{pat},y_{pat}) are defined by $x_{\alpha_i}=d_{\alpha_i}\cos(\theta_i)$, $y_{\alpha_i}=d_{\alpha_i}\sin(\theta_i)$, $x_{pat}=\sum_{\alpha_i\in P}x_{\alpha_i}$, $y_{pat}=\sum_{\alpha_i\in P}y_{\alpha_i}$, where P denotes the local patch.

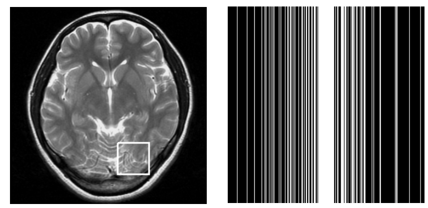

(a) **(b)**

Fig. 2 T2 weighted MR image (a) and Cartesian sampling pattern with 30% k-space data acquired (b).

Results and discussion

The MR image used for simulations is T_2 weighted and obtained from a 1.5T GE MRI scanner, as shown in Fig. 2 (a). À trous WT with spline biorthogonal filters and four decomposition levels is used as the sparsifying transform. Cartesian sampling pattern [1] with 30% measurements are acquired, as shown in Fig. 2 (b). Relative ℓ_2 norm error (RLNE) is adopted to evaluate the normalized error presented in the reconstruction compared with the fully sampled MR image. The proposed algorithm is compared with the fast iterative soft-thresholding algorithm (FISTA) [2], reweighted ℓ_1 norm (RWL1) minimization algorithm [3], and edge correlation incorporated algorithm (ECIA) [4]. The comparison is given in Fig. 3. We can observe that edges obtained by the proposed method are much clearer than the other three methods. The proposed method also yields lowest RLNE among the four methods. In addition, to test the performance of different methods under different sampling rates, we give the curve of RLNE versus sampling rate in Fig. 4. The image used in this trial is the same as Fig. 2 (a), with Cartesian sampling scheme employed. The curves in Fig. 4 indicates that, when the acquired k-space data grows to 25%-35%, the RLNEs for the proposed method fall between 0.04-0.07, under which we think reconstruction quality is relatively acceptable. However, RWL1 and ECIA achieve RLNEs of the same level with nearly 35%-40% k-space measurements.

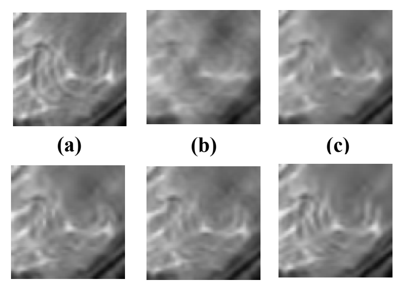

(a) **(b)** **(c)**

(d) **(e)** **(f)**

Fig. 3 Zoom-in reconstructed regions labeled in Fig. 2 (a). (a)-(f) are fully sampled image, zero-filling image, reconstructions by FISTA, RWL1, ECIA, and the proposed method, respectively. The RLNEs for (b)-(f) are 0.247, 0.096, 0.092, 0.084, and 0.066 to the fully sampled image.

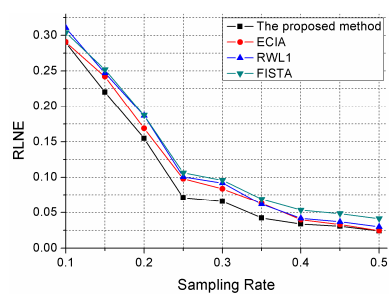

Fig. 4 RLNE curves obtained by different methods with different sampling rates using the Cartesian sampling scheme.

Acknowledgment

This work was supported by NNSF of China (10974164, 11174239). We would like to thank Rice University for sharing the rice wavelet toolbox.

References

[1] Lustig M, et al. *Magn. Reson. Med.* 58 (2007) 1182–1195.
[2] Beck A, et al. *SIAM J. Imaging Sci.* 2 (2009) 183–202.
[3] Candès E, et al. *J. of Fourier Analysis and Applications*, 14 (2008) 877–905.
[4] Hu C, et al. *Magn. Reson. Imaging*, 29 (2011) 907–915.